PLASMA DIAGNOSTICS

IMPROVING THE EFFICIENCY OF LASER ACCELERATION OF PROTONS USING ULTRA-THIN TARGETS

© 2025 A. A. Bushukhin*, K. V. Safronov, S. A. Gorokhov, V. A. Flegentov, D. O. Zamuraev, A. L. Shamraev, S. F. Kovaleva, N. A. Fedorov, A. V. Potapov

FSUE "RFNC-VNIITF named after academician E.I. Zababakhin", Snezhinsk, Russia

**e-mail: dep5@vniitf.ru*

Received November 29, 2024

Revised January 09, 2025

Accepted January 12, 2025

Abstract. The paper presents the results of laser acceleration of protons from 6 μm-thick aluminum targets and 100 nm-thick ultrathin diamond-like carbon films irradiated with femtosecond laser pulses with a peak intensity of up to 5·1020 W/cm2. It is shown that decreasing the target thickness from 6 μm to 100 nm does not lead to a significant change in the maximum proton energies, but contributes to an increase in the angular yield and the laser energy conversion coefficient. This effect is due to an increase in the number of protons in the low-energy part of the spectra, which is reflected in a twofold increase in the conversion coefficient.

Keywords: *ultrashort laser pulses, relativistic intensity, laser-plasma acceleration of protons, time-of-flight method, double plasma mirror*

DOI: 10.31857/S03672921250101e8

1. INTRODUCTION

Modern powerful laser installations with ultra-short pulse durations make it possible to generate radiation that, when interacting with matter, is capable of creating quasi-electrostatic fields with intensities exceeding 1 TV/m [1]. This value is more than 10^4times exceeds the field strengths realized in modern radio-frequency charged particle accelerators. In this regard, many researchers are considering the possibility of using ultrashort lasers to create compact accelerators of the next generation. It is assumed that such accelerators will find application in various scientific fields, from studies of warm dense plasma [2, 3] to modeling beams of charged particles present in outer space [4].

At laser radiation intensities of 10^{19}-10^{21} W/cm^2 with pulse durations of tens of femtoseconds, ion acceleration to energies of ~40 MeV/nucleon occurs in a thin Debye layer of charge separation

normal to the target (*target normal sheath acceleration*, *TNSA*) [5, 6]. This layer is formed by a cloud of "hot" electrons accelerated by laser radiation from the pre-plasma formed on the front side of the targets. For targets less than 100 nm thick, other mechanisms begin to predominate [7-10], allowing the production of laser-accelerated proton beams with energies up to 100 MeV [11-15].

The use of ultrathin targets requires strict control over the ratio of the main laser pulse intensity to the intensity of spontaneous amplified luminescence, i.e., the contrast level of the laser system. This ratio should be no worse than 10^{10}:1 at 1 ps before the arrival of the main pulse. Otherwise, the irradiated target may be destroyed before the arrival of the main pulse.

This paper presents experimental results of proton acceleration by laser pulses with peak intensities exceeding 10^{20} W/cm^2 from targets with thicknesses of 6 μm and 100 nm. A weak dependence of maximum proton energies on the material and thickness of the irradiated targets is shown. With a laser energy of E_{las} = 0.8 J, the maximum proton energies reach ~5 MeV. An increase in the angular yield of protons was demonstrated when using diamond-like carbon films with a thickness of 100 nm as targets due to an increase in the number of protons in the low-energy part of the spectrum.

2. EXPERIMENTAL SETUP

The research was performed on a Ti:Sa femtosecond laser system of the 100 TW class. Laser pulses with a wavelength of 800 nm, energy up to 2 J, and duration of 27±2 fs were directed normal to the target by means of an off-axis parabolic mirror *f/2.5* with a focal length of 160 mm. The peak intensity of laser radiation on the target surface reached $5 \cdot 10^{20}$ W/cm^2 with 50% of the energy contained in a focal spot with a diameter of 3 μm. The experimental setup is shown in Fig. 1.

The experiments used targets made of aluminum foils with a thickness of 6 μm, as well as ultrathin films of *diamond-like carbon, DLC* with a thickness of 100 nm. The choice of thickness for the ultrathin targets was determined by technological limitations in their manufacturing. Figure 2 shows the scheme of mounting targets on an aluminum holder. To guide the working radiation onto the surface of targets located on the same radius, reflecting mirrors were used with the alignment laser.

In experiments on proton generation from targets with a thickness of 100 nm, a system based on a double plasma mirror was used, which improved the temporal contrast of the laser facility by 10^4 times [16-20]. It is based on the effect of a self-induced plasma shutter. Laser radiation is focused on a reflective surface made of a dielectric material with a low laser reflection coefficient of ~10^{-3}. When interacting with a pre-pulse with an intensity exceeding the ionization threshold for the given material,

a thin plasma layer forms on the mirror surface a few picoseconds before the arrival of the main laser pulse. If the electron density of the formed solid-state plasma coincides with the critical density for the wavelength of the incident laser radiation, there is a sharp increase in the reflection coefficient to values close to 1. As a result, the contrast of the laser facility increases by a value equal to the ratio of the reflection coefficients of plasma and dielectric. Typical schemes of this system are widely described in the literature [16-20].

One of the disadvantages of the contrast enhancement system used is its relatively low energy efficiency, which characterizes the fraction of the incident laser radiation energy reflected from the mirror. This effect is due to scattering and absorption of laser radiation by the formed plasma. In the described experiments, the energy efficiency of the double plasma mirror system reaches 60%. It is also worth noting that experiments on laser-plasma acceleration of protons from aluminum foils with a thickness of 6 μm were conducted without using this system, i.e., with a lower level of laser radiation contrast.

One of the most common methods for registering laser-accelerated proton beams is the use of radiochromic films (*Radiochromic Films, RCF*) [6, 11-14, 21, 22]. However, it has a number of significant disadvantages, such as single-use films and the need to open the vacuum chamber after each shot to replace the recording detector.

Within the framework of the conducted research, the time-of-flight method was applied for proton beam registration. A semiconductor silicon photodiode was used as a detector in the spectrometer. The advantages of this method are the promptness of obtaining experimental data without the need to break the vacuum, as well as simplicity in processing them.

The time-of-flight spectrometer (TOF) was installed normal to the target plane at a distance of 1519 mm. To protect against heavy ions, the detector's input aperture with a diameter of 1 mm was covered with a 6 μm thick aluminum filter, cutting off protons with energy less than 600 keV. The signals from the TOF were recorded using an oscilloscope with a sampling rate of 5 GS/s. The temporal resolution of the spectrometer was (3.3±0.1) ns, which corresponds to an energy resolution of 0.6 MeV for protons with energies of 5 MeV.

3. DISCUSSION OF EXPERIMENTAL RESULTS

Figure 3 shows characteristic proton spectra reconstructed from TOF signals. Dependencies of maximum energies E_{max} and angular yield F_p of protons on the laser radiation energy were also obtained for 6 μm thick Al targets, as well as ultrathin films with a thickness of 100 nm (Figures 4

and 5). The values of the angular yield F_p were calculated by integrating the proton spectra over energy (from 0.6 MeV to E_{max})

$$F_p = \int_{0.6}^{E_{max}} \frac{d^2N(E)}{dEd\Omega} dE, \quad (1)$$

where $d^2N/(dEd\Omega)$ is the differential energy spectrum normalized to the detector's solid angle, E is the proton energy (MeV).

With a laser energy on target of ~1.6 J, proton beams with energies up to (8.4±1.5) MeV and an angular yield of $\sim 10^{11}$ sr^{-1} were obtained. In experiments with ultrathin targets, the laser energy on target did not exceed 0.86 J. As a result, protons with energies up to (5.3±0.7) MeV and an angular yield of $6 \cdot 10^{10}$ sr^{-1} were registered. In previous experiments, we demonstrated the independence of proton parameters from the material of the irradiated target with similar atomic numbers Z [23], which allows for direct comparison of the obtained results.

It is worth noting that the dependence of maximum proton energies on laser energy for both types of targets has a nearly linear character $E_{max} \sim (E_{las})^{0.8}$, and is in agreement with the results of other authors [24, 25].

As seen from Fig. 4, decreasing the target thickness did not change the maximum proton energies. This effect can be explained by different contrast levels of the laser radiation. In experiments with aluminum foils, a lower contrast level leads to the formation of a thin preplasma layer on the front surface of the targets, which increases the efficiency of laser energy absorption by hot electrons that form an accelerating layer on its rear side [26]. Let's compare the maximum proton energies recorded in experiments with values given by the classical theory of plasma expansion into vacuum [27]

$$E_{max} = 2Z_i T_h \left[\ln(2\tau)\right]^2, \quad (2)$$

where $Z_i = 1$ is the proton charge, T_h is the hot electron temperature, which is estimated from the ponderomotive potential $T_h = mc^2\left(\sqrt{1+a_0^2/2}-1\right) \approx 3.9$ MeV [28], where $a_0 = 12$ is the dimensionless amplitude of the laser field for peak intensity in our experiments. The value τ can be calculated as

$$\tau = \frac{t_{acc}}{\sqrt{2e_N}} \sqrt{\frac{4\pi Z_i n_{e0} e^2}{m_i}} = 1.373. \quad (3)$$

Here $t_{acc} = 1.3\ t_{las} = 35$ fs [29] is the proton acceleration time, $e_N = 2.718$, e is the electron charge, m_i is the proton mass, n_{e0} is the initial electron density on the rear surface of the target

$$n_{e0} = \frac{\eta E_{las}}{ct_{las}\pi r^2 k_B T_h} = 4.8 \cdot 10^{21}\ \text{см}^{-3}, \qquad (4)$$

where $\eta = 0.5$ is the efficiency of energy absorption by electrons, $E_{las} = 1$ J is the laser pulse energy in the focal spot with diameter $r_{las} = 3$ μm, r is the radius of the proton source, which is calculated by the formula $r = r_{las} + d\tan(10^\circ)$ [29], $d = 6$ μm is the target thickness, $t_{las} = 27$ fs is the laser pulse duration, k_B is the Boltzmann constant.

Substituting the obtained values into formula (2), we get an estimate of the maximum proton energies at the level of ~8 MeV at peak laser intensity. The obtained value is in agreement with the experimental data shown in Fig. 4. Thus, it can be concluded that in the case of aluminum targets without the use of a plasma mirror system, charge separation effects on the rear surface of the targets play a dominant role in the proton acceleration process.

In the case of ultrathin targets, a higher contrast level leads to the formation of a denser preplasma layer, which prevents efficient absorption of laser energy by electrons. Comparable maximum proton energies in this case are achieved through a two-stage acceleration: Coulomb explosion on the front surface of the target and *TNSA* on the rear surface. The first acceleration mechanism is realized due to the formation of a positively charged cavity under the action of light pressure, which pushes out electrons [30-32]. The thickness of this cavity is determined by the balance between Coulomb forces and light pressure, which ultimately leads to Coulomb explosion and proton acceleration. Upon reaching the rear surface of the target, further acceleration of protons occurs normal to the target due to the *TNSA* mechanism.

From the data shown in Fig. 5, it can be seen that decreasing the thickness of the irradiated targets led to an increase in the angular yield of protons by up to 5 times. This result is due to the increased number of protons with energies less than 2.5 MeV. When comparing the obtained results, the assumption is used that the angular aperture of the proton beam remains unchanged when the target thickness is reduced to 100 nm. The growth of the angular yield of protons without changing their maximum energies with decreasing target thickness was previously observed in our experiments on a picosecond laser system [33].

The observed effect may be due to partial destruction of ultrathin targets as a result of the implementation of a two-stage acceleration mechanism, accompanied by Coulomb explosion on the

front surface of the target. A similar result was obtained in [34] when irradiating aluminum targets with a thickness of 500 nm.

The conversion coefficient of laser energy into proton energy was calculated K_{conv}, as the ratio of the energy content in the proton beam to the energy of the laser pulse:

$$K_{conv} = \left(E_{las}\right)^{-1} \int_{0.6}^{E_{\max}} E \frac{d^2 N(E)}{dE d\Omega} dE. \quad (5)$$

Similar to formula (1), the integration of spectra was carried out over proton energies in the range from 0.6 MeV to $E_{\max}$. For the laser pulse energy on the target $E_{las} \sim 0.7$ J, the conversion coefficient of laser energy into protons with energies above 600 keV reaches $K_{conv} = 1.13\%$/sr with an energy content in the proton beam of 8 mJ/sr when irradiating ultrathin targets and $K_{conv} = 0.48\%$/sr with an energy content in the proton beam of 3.4 mJ/sr for the case of 6 μm Al.

4. CONCLUSION

Experiments on laser-plasma proton acceleration from 6 μm thick aluminum targets and 100 nm thick diamond-like carbon films were conducted at the femtosecond laser facility with laser intensities up to $5 \cdot 10^{20}$ W/cm². Proton beams with energies up to 8.4 MeV and angular yield of $\sim 10^{11}$ sr^{-1} were registered. When reducing the target thickness from 6 μm to 100 nm, no increase in maximum proton energies was observed. This is explained by differences in the laser contrast level and acceleration mechanisms. In the case of ultrathin targets, proton acceleration occurs in two stages: Coulomb explosion on the front surface of the target and subsequent acceleration by the *TNSA* mechanism on its rear side.

Irradiation of ultrathin targets led to an increase in the angular yield of protons by up to 5 times due to the growth of their number in the low-energy part of the spectrum. The observed effect can be explained by partial destruction of targets at the initial stage of proton acceleration. The conversion coefficient of laser energy into proton energy reaches 0.48%/sr for 6 μm thick targets and 1.13%/sr for 100 nm thick diamond-like carbon films with comparable laser pulse energy of approximately 0.7 J.

Proton beams characterized by increased content of low-energy particles may be of interest for studies of submicron thickness material properties under isochoric heating to temperatures of about 1-10 eV [2, 3].

CONFLICT OF INTERESTS

The authors declare that they have no conflict of interest.

REFERENCES

1. *Badziak J.* // J. Phys.: Confer. Ser. 2017. V. 959. P. 012001. Doi: 10.1088/1742-6596/959/1/012001.
2. *Feldman S., Dyer G., Kuk D., Ditmire T.* // Phys. Rev. E. 2017. V. 95. P. 031201. Doi: 10.1103/PhysRevE.95.031201.
3. *Dyer G.M., Bernstein A.C., Cho B.I., Osterholz J., Grigsby W., Dalton A., Shepherd R., Ping Y., Chen H., Widmann K., Ditmire T.* // Phys. Rev. Lett. 2008. V. 101. P. 015002.

Doi: 10.1103/PhysRevLett.101.015002.

4. *Hidding B., Karger O., Königstein T., Pretzler G., Manahan G.G., McKenna P., Gray R., Wilson R., Wiggins S.M., Welsh G.H., Beaton A., Delinikolas P., Jaroszynski D.A., Rosenzweig J.B., Karmakar A., Ferlet-Cavrois V., Costantino A., Muschitiello M., Daly E.* // Sci. Rep. 2016. V. 7. P. 42354. Doi: 10.1038/srep42354.
5. *Wilks S.C., Langdon A.B., Cowan T.E., Roth M., Singh M., Hatchett S., Key M.H., Pennington D., MacKinnon A., Snavely R.A* // Phys. Plasmas. 2001. V. 8. P. 542. Doi: 10.1063/1.1333697.
6. *Poole P.L., Obst L., Cochran G.E., Metzkes J., Schlenvoigt H.-P., Prencipe I., Kluge T., Cowan T., Schramm U., Schumacher D.W., Zeil K.* // New J. Phys. 2018. V. 20. P. 013019. Doi: 10.1088/1367-2630/aa9d47.
7. *Esirkepov T., Borghesi M., Bulanov S.V., Mourou G., Tajima T.* // Phys. Rev. Lett. 2004. V. 92. P. 175003. Doi: 10.1103/PhysRevLett.92.175003.
8. *d'Humires E., Lefebvre E., Gremillet L., MalkaV.* // Phys. Plasmas. 2005. V. 12. P. 062704. Doi: 10.1063/1.1927097.
9. *Yin L., Albright B.J., Hegelich B.M., Fernandez J.C.* // Laser Part. Beams. 2006. V. 24. P. 291. Doi: 10.1017/S0263034606060459.
10. *Macchi A., Borghesi M., Passoni M.* // Rev. Mod. Phys. 2013. V. 85. P. 751.

Doi: 10.1103/RevModPhys.85.751.

11. *Higginson A., Gray R.J., King M., Dance R.J., Williamson S.D.R., Butler N.M.H., Wilson R., Capdessus R., Armstrong C., Green J.S., Hawkes S.J., Martin P., Wei W.Q., Mirfayzi S.R., Yuan*

X.H., Kar S., Borghesi M., Clarke R.J., Neely D., McKenna P. // Nature Commun. 2018. V. 9. P. 724. Doi: 10.1038/s41467-018-03063-9.

12. *Dover N.P., Ziegler T., Assenbaum S., Bernert C., Bock S., Brack F.E., Cowan T.E., Ditter E.J., Garten M., Gaus L., Goethel I., Hicks G.S., Kiriyama H., Kluge T., Koga J.K., Kon A., Kondo K., Kraft S., Kroll F., Lowe H.F., Metzkes N.J., Miyatake T., Najmudin Z., Puschel T., Rehwald M., Reimold M., Sakaki H., Schlenvoigt H.P., Shiokawa K., Umlandt M.E.P., Schramm U., Zeil K., Nishiuchi M.* // Light Sci. Appl. 2023. V. 12. P. 71. Doi: 10.1038/s41377-023-01083-9.
13. *Wagner F., Deppert O., Brabetz C., Fiala P., Kleinschmidt A., Poth P., Schanz V.A., Tebartz A., Zielbauer B., Roth M., Stohlker T., Bagnoud V.* // Phys. Rev. Lett. 2016. V. 166. P. 205002. Doi: 10.1103/PhysRevLett.116.205002.
14. *Liu Z., Gao Y., Wu Q., Pan Z., Liang Y., Song T., Xu T., Shou Y., Zhang Y., Chen H., Han Q., Hua C., Chen X., Xu S., Mei Z., Wang P., Peng Z., Zhao J., Chen S., Zhao Y., Yan X., Ma W.* // Phys. Plasmas. 2024. V. 31. P. 053106. Doi: 10.1063/5.0195634.
15. *Ziegler T., Gothel I., Assenbaum S., Bernert C., Brack F.E., Cowan T.E., Dover N.P., Gaus L., Kluge T., Kraft S., Kroll F., Metzkes-Ng J., Nishiuchi M., Prencipe I., Puschel T., Rehwald M., Reimold M., Schlenvoigt H.P., Umlandt M.E.P., Vescovi M., Schramm U., Zeil K.* // Nature Phys. 2024. V. 20. P. 1211. Doi: 10.1038/s41567-024-02505-0.
16. *Levy A., Ceccotti T., D'Oliveira P., Reau F., Perdrix M., Quere F., Monot P., Bougeard M., Lagadec H., Martin P.* // Optics Letters. 2007. V. 32. P.310. Doi: 10.1364/ol.32.000310.
17. *Kim I.J., Choi I.W., Janulewicz K.A., Lee J.* // J. Optical Society of Korea. 2009. V. 13(1). P. 15. Doi: 10.3807/JOSK.2009.13.1.015.
18. *Du D., Liu X., Korn G., Squier J., Mourou G.* // Appl. Phys. Lett. 1994. V. 64. P. 3071. Doi: 10.1063/1.111350.
19. *Kim I.J., Choi I., Lee S.K., Janulewicz K.A., Sung J.H., Yu T. J., Kim H.T., Yun H., Jeong T.M., Lee J.* // Appl. Phys. B. 2011. V. 104(1). P. 81. Doi: 10.1007/s00340-011-4584-2.
20. *Mikhailova J.M., Buck A., Borot A., Schmidt K., Sears C., Tsakiris G.D., Krausz F., Veisz L.* // Opt. Lett. 2011. V. 36. P. 3145. Doi: 10.1364/OL.36.003145.
21. *Higginson A., Wilson R., Goodman J., King M., Dance R.J., Butler N.M.H., Armstrong C.D., Notley M., Carroll D.C., Fang Y., Yuan X.H., Neely D., Gray R.J., McKenna P.* // Plasma Phys. Control. Fusion. 2021. V. 63. P. 114001. Doi: 10.1088/1361-6587/ac2035.
22. *Padda H., King M., Gray R.J., Powell H.W., Gonzalez-Izquierdo B., Stockhaussen L.C., Wilson R., Caroll D.C., Dance R.J., MacLellan D.A., Yuan X.H., Butler N.M.H., Capdessus R., Borghesi M., Neely D., McKenna P.* // Phys. Plasmas. 2016. V. 23. P. 063116. Doi: 10.1063/1.4954654.

23. *Safronov K.V., Vikhlyaev D.A., Vladimirov A.G., Gavrilov D.S., Gorokhov S.A., Kakshin A.G., Loboda E.A. Lykov V.A., Mokicheva E.S., Potapov A.V., Pronin V.A., Saprykin V.N., Tolstoukhov P.A., Chefonov O.V., Chizhkov M.N.* // Physics of Plasma. 2010. V. 36. P. 478. Doi: 10.1134/S1063780X10050119.

24. *Zeil K., Kraft S.D., Bock S., Bussmann M., Cowan T.E., Kluge T., Metzkes-Ng J., Richter T., Sauerbrey R., Schramm U.* // New J. Phys. 2010. V. 12. P. 045015. Doi: 10.1088/1367-2630/12/4/045015.

25. *Fourmaux S., Buffechoux S., Albertazzi B., Capelli D., Levy A., Gnedyuk S., Lecherbourg L., Lassonde P., Payeur S., Anitici P., Pepin H., Marjoribanks R.S., Fuchs J., Kieffer J.C.* // Phys. Plasmas. 2013. V. 20. P. 013110. Doi: 10.1063/1.4789748.

26. *Carrie M., Lefebvre E., Flacco A., Malka V.* // Nuclear Instrum. Methods Phys. Res. A. 2010. V. 620(1). P. 36-40. Doi: 10.1016/j.nima.2010.01.056.

27. *Mora P.* // Phys. Rev. Lett. 2003. V. 90. P. 185002. Doi: 10.1103/PhysRevLett.90.185002.

28. *Wilks S.C., Kruer W.L.* // IEEE J. Quantum Electron. 1997. V. 33(11). P. 1954. Doi: 10.1109/3.641310.

29. *Daido H., Nishiuchi M., Pirozhkov A.S.* // Reports Prog. Phys. 2012. V. 75. P. 056401. Doi: 10.1088/0034-4885/75/5/056401.

30. *Levy D., Andriyash I.A., Haessler S., Kaur J., Ouillé M., Flacco A., Kroupp E., Malka V., Lopez-Martens R.* // Phys. Rev. Accelerated Beams. 2022. V. 25. P. 093402. Doi: 10.1103/PhysRevAccelBeams.25.093402.

31. *Bychenkov V.Yu.,Singh P.K., Ahmed H., Kakolee K.F., Scullion C., Jeong T.W., Hadjisolomou P., Alejo A., Kar S., Borghesi M., Ter-Avetisyan S. //* Phys. Plasmas. 2017. V. 24. P. 010704. Doi: 10.1063/1.4975082.

32. *Ter-Avetisyan S., Varmazyar P., Singh P.K., Son J.G., Fule M., Bychenkov V.Yu., Farkas B., Nelissen K., Mondal S., Papp D., Borzsonyi A., Csontos J., Lecz Z., Somoskoi T., Toth L., Andriy V., Margarone D., Necas A., Mourou G., Szabo G., Osvay K.* // Plasma Phys. Control. Fusion. 2023. V. 65. P. 085012. Doi: 10.1088/1361-6587/acde0a.

33. *Safronov K.V., Vikhlyaev D.A., Vladimirov A.G., Gavrilov D.S., Gorokhov S.A., Kakshin A.G., Loboda E.A., Lykov V.A., Mokicheva E.S., Potapov A.V., Pronin V.A., Saprykin V.N., Tolstoukhov P.A., Chefonov O.V., Chizhkov M.N.* // JETP Letters. 2008. V. 88. P. 830. Doi: 10.1134/S0021364008230033.

34. *Green J.S., Robinson A.P.L., Booth N., Carroll D.C., Dance R.J., Gray R.J., MacLellan D.A., McKenna P., Murphy C.D., Rusby D., Wilson L.* // Appl. Phys. Lett. 2014. V. 104. P. 214101. Doi: 10.1063/1.4879641.

FIGURE CAPTIONS

Рис. 1. Experimental setup scheme.

Рис. 2. Scheme for mounting targets on an aluminum disk.

Рис. 3. Characteristic proton spectra in experiments with aluminum targets and ultrathin films.

Рис. 4. Dependence of maximum proton energies on laser energy at the target.

Рис. 5. Dependence of angular yield of protons with energies above 600 keV on laser energy at the target.

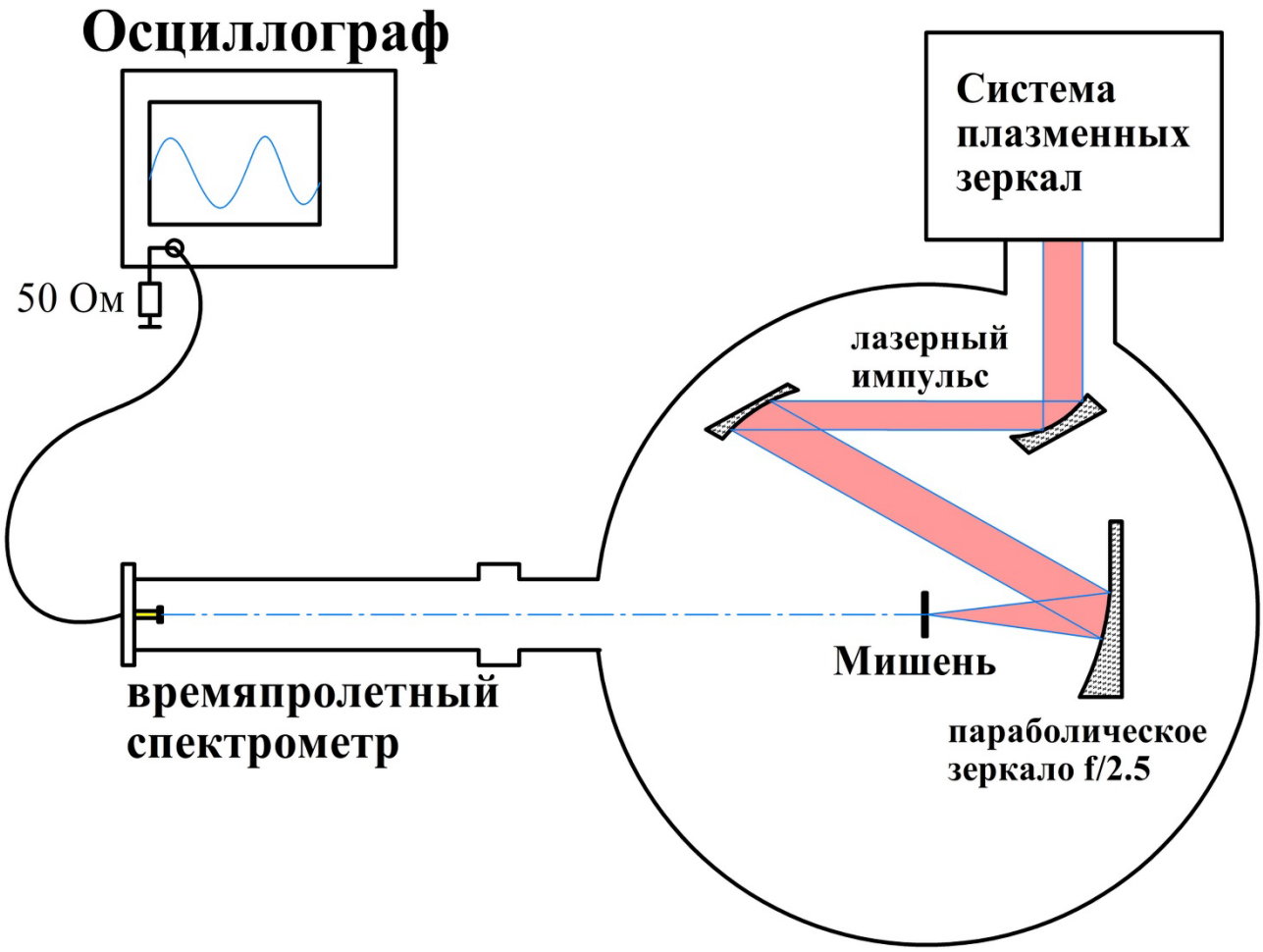
Осциллограф
50 Ом
Система плазменных зеркал
лазерный импульс
Мишень
времяпролетный спектрометр
параболическое зеркало f/2.5

Fig. 1.

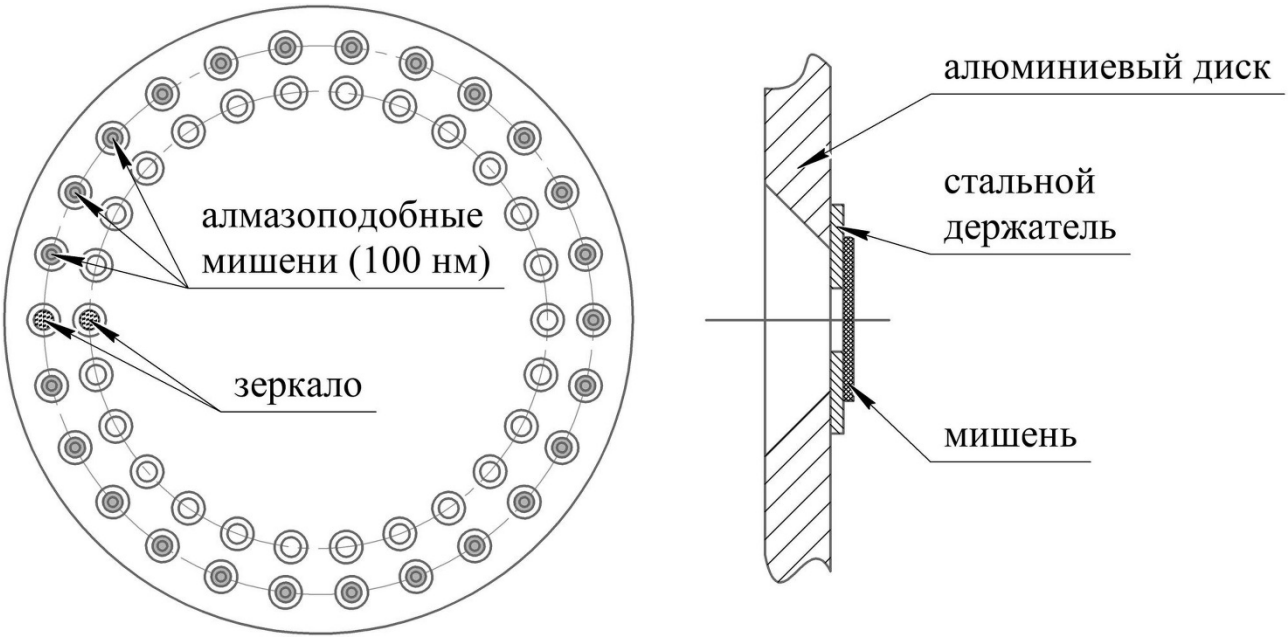
алмазоподобные мишени (100 нм)
зеркало
алюминиевый диск
стальной держатель
мишень

Fig. 2.

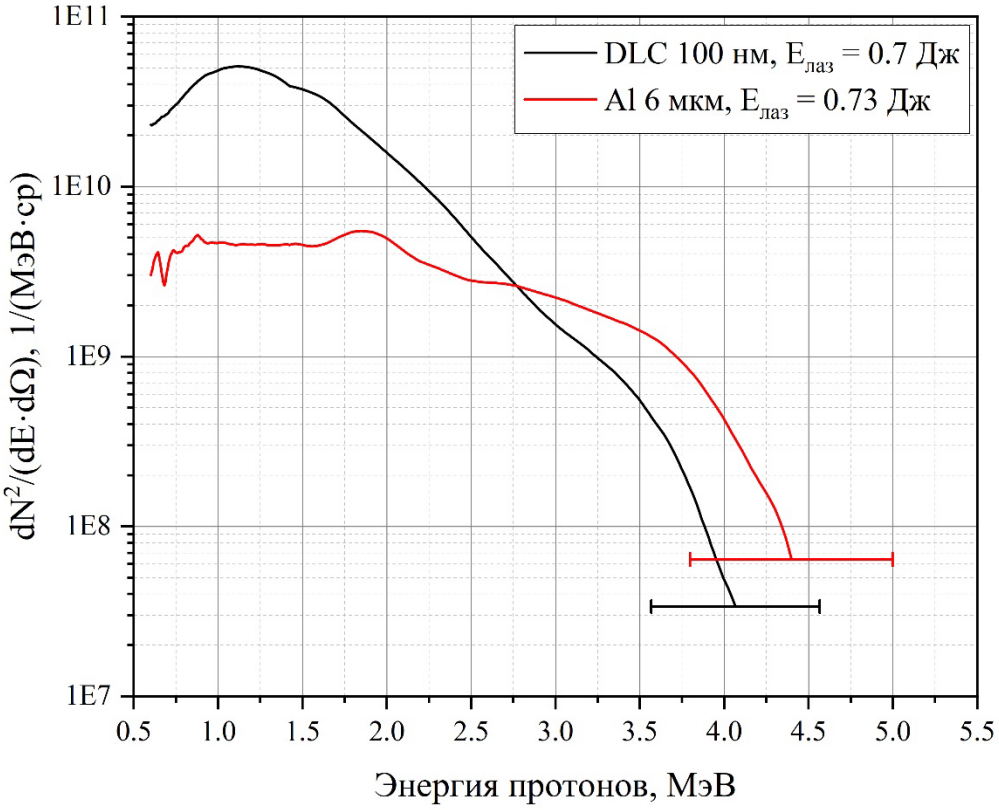
DLC 100 нм, Eлаз = 0.7 Дж
Al 6 мкм, Eлаз = 0.73 Дж
1E11
1E10
1E9
1E8
1E7
dN²/(dE·dΩ), 1/(МэВ·ср)
0.5
1.0
1.5
2.0
2.5
3.0
3.5
4.0
4.5
5.0
5.5
Энергия протонов, МэВ

Fig. 3.

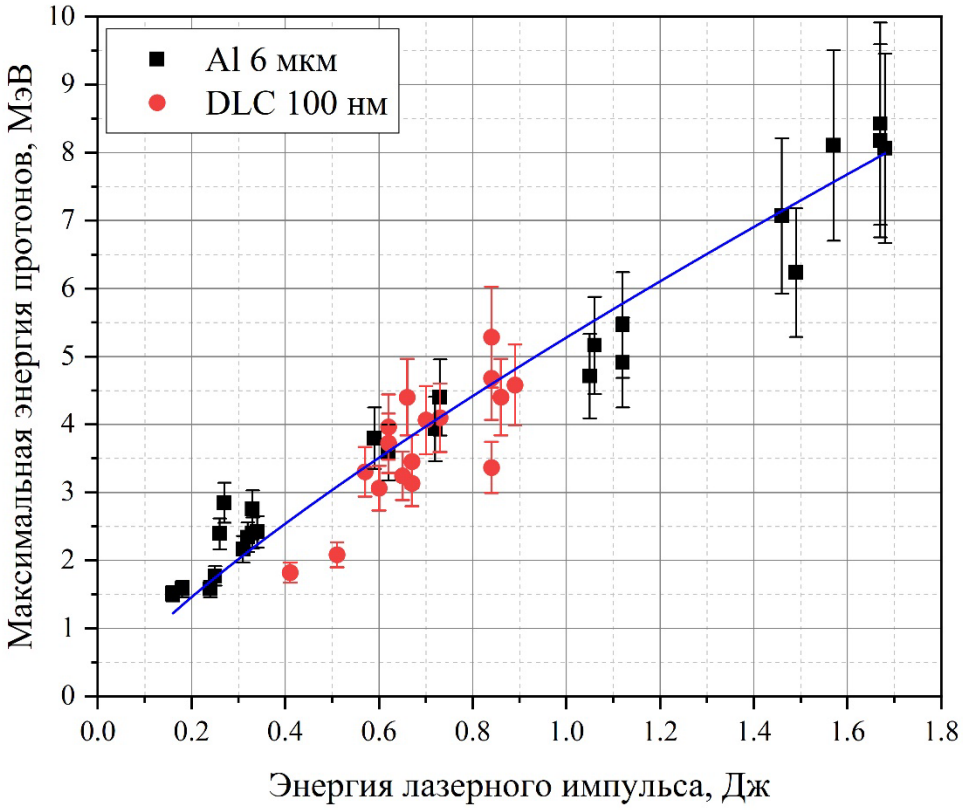
Al 6 мкм
DLC 100 нм
Максимальная энергия протонов, МэВ
Энергия лазерного импульса, Дж
0
1
2
3
4
5
6
7
8
9
10
0.0
0.2
0.4
0.6
0.8
1.0
1.2
1.4
1.6
1.8

Fig. 4.

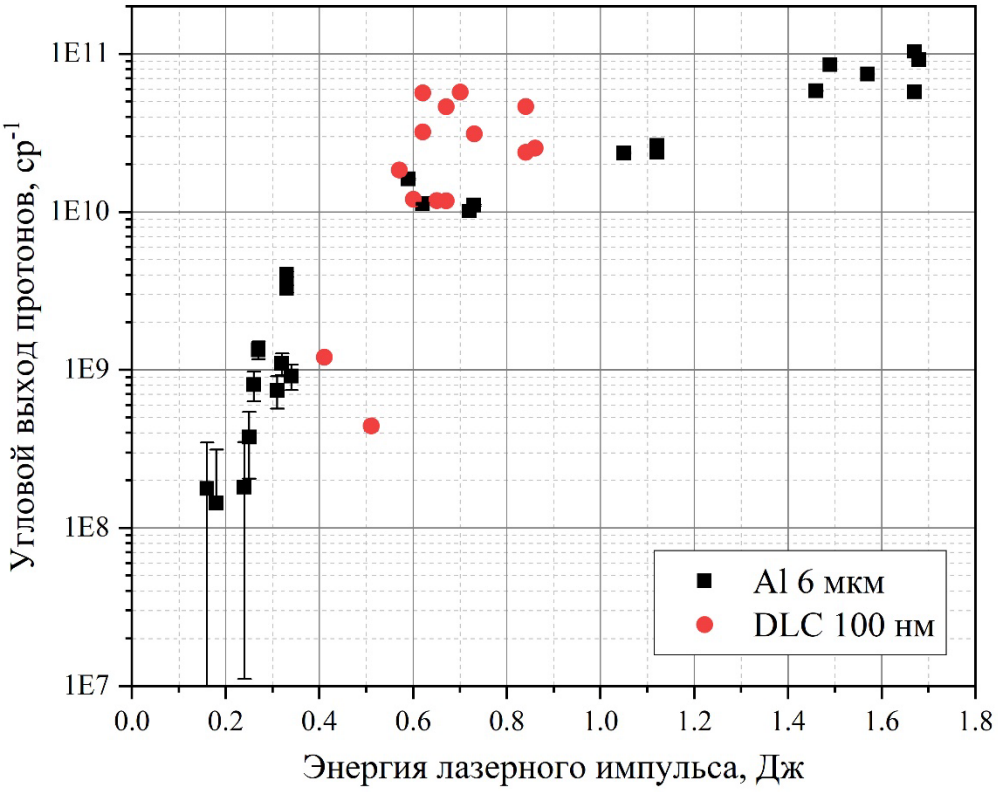
1E11
1E10
1E9
1E8
1E7
Угловой выход протонов, ср-1
0.0
0.2
0.4
0.6
0.8
1.0
1.2
1.4
1.6
1.8
Энергия лазерного импульса, Дж
Al 6 мкм
DLC 100 нм

Fig. 5.